Electronic Supplementary Information

A Strategy of Asymmetric Local Structure Based on Mesoporous MoO_2 toward Efficient Electrocatalysis

Xinyue Zheng,‡[a] Wenjing Wang,‡[a] Gan Jia,*[b] Zhaosheng Li*[a] and Zhigang Zou[a]

a. *Collaborative Innovation Center of Advanced Microstructures, National Laboratory of Solid State Microstructures, College of Engineering and Applied Sciences, Nanjing University, Nanjing, 210093 China.*
E-mail: zsli@nju.edu.cn

b. *College of Material, Chemistry and Chemical Engineering, Hangzhou Normal University, Hangzhou, 311121 China.*
E-mail: gjia@hznu.edu.cn

‡ X. Zheng and W. Wang contributed equally to this work.

Experimental Section

Chemicals:

Phosphomolybdic acid hydrate ($H_3PMo_{12}O_{40}$) was obtained from Sigma-Aldrich Co., Ltd. KIT-6 was purchased by XFNANO Co., Ltd. Ferric chloride ($FeCl_3 \cdot 6H_2O$), cobalt chloride ($CoCl_2 \cdot 6H_2O$), nickel chloride ($NiCl_2 \cdot 6H_2O$), and sodium hydroxide (NaOH) were purchased from Sinopharm Chemical Reagent Co., Ltd. Deionized water used in this experiment presented a resistivity of 18 MΩ. All the chemicals were utilized without further purification.

Preparation of Meso-MoO_2 and doping samples:

$H_3PMo_{12}O_{40}$ (2 g) and KIT-6 (0.5 g) were mixed in 5 mL ethanol under room temperature with vigorously stirring. After the evaporation of solvent, the powders were transfer to an alumina crucible and then heated in a tube furnace at 500 ℃ under the atmosphere of 95%Ar/5%H_2. After heating for 5 h, the obtained composite was treated by NaOH solution to remove the KIT-6 template and deionized water was used to rinse the samples. Finally, Meso-MoO_2 were obtained after being dried at 60 °C for 12 h. M-MoO_2 (M=Fe, Co, Ni) with different doping concentrations were synthesized by similar methods. Different atomic ratios of $FeCl_3 \cdot 6H_2O$, $CoCl_2 \cdot 6H_2O$, $NiCl_2 \cdot 6H_2O$ were mixed with $H_3PMo_{12}O_{40}$ and KIT-6, respectively, based on the doping concentration (0.5 at.%~3.0 at.%). The following steps are the same as the method of preparing Meso-MoO_2.

Preparation of Bulk-MoO_2 and doping samples:

Approaches are similar with the synthesis of mesoporous ones except for the lack of KIT-6 when preparing the precursor and the subsequent step of removing KIT-6 template.

Characterizations:

X-ray diffraction (XRD) patterns were measured by a Rigaku UltimaIII diffractometer (Japan) with Cu Ka radiation (1.54178 Å) at 40 kV and 40 mA. Scanning electron microscopy (SEM) was collected by using Carl Zeiss SMT AG (Germany). Transmission electron microscopy (TEM) was performed by JEOL JEM-

2100 (Japan). X-ray photoelectron spectroscopy (XPS) measurements were carried out on a PHI 5000 VersaProbe instrument (Japan) using Al Kα monochromatic X-ray radiation source. Nitrogen sorption isotherms were collected on TriStar 3000 (the United States) at 77 K.

Electrochemical measurements:

OER electrochemical experiments were carried out by using a standard three-electrode system at room temperature on a CHI 760D (CH Instrument, Shanghai, China) electrochemical workstation. The working electrode is the rotating disk electrode coated with catalyst. A platinum wire and Hg/HgO electrode were used as counter electrode and reference electrode, respectively. The electrolyte was O_2-saturated 1.0 M KOH. The electrode potential vs. Hg/HgO can be converted to the reversible hydrogen electrode (RHE), based on the Nernst equation: $E_{RHE} = 0.098\ V + 0.059 \times pH + E_{measured}$. Working electrode can be prepared by the following method. 5 mg catalyst, 230 μL ethanol, 730 μL deionized water, and 40 μL Nafion (5 wt. %) were mixed by ultrasonicating for 20 min. Afterward, 4 μL of the obtained catalyst ink was coated on glass carbon (GC) electrode. The loading is about 0.287 mg cm^{-2}. 1%Ni-Meso-MoO_2/NF is prepared with nickel foam (NF) as support by similar method, and the loading is about 3 mg cm^{-2}.

Density functional theory (DFT) calculation details:

All our calculations in this study are performed using the Vienna ab initio simulation package (VASP)[1,2], which employs the spin-polarized DFT method. The generalized gradient approximation (GGA)[3] in the scheme of Perdew-Bueke-Ernzerhof (PBE)[4] is used for the exchange correlation functional. The projection augmented wave (PAW)[5] pseudo potential was used to describe the core and the valence electrons. The cutoff energy is 520 eV, which is high enough to ensure that no Pulay stresses occur within the cell during geometry relaxations in all materials. And a 7×5×5 k-point sampling in reciprocal space was used for MoO_2. Geometry relaxations are carried out until the residual forces on each ion converged to be smaller than 2E-05 eV/Å.

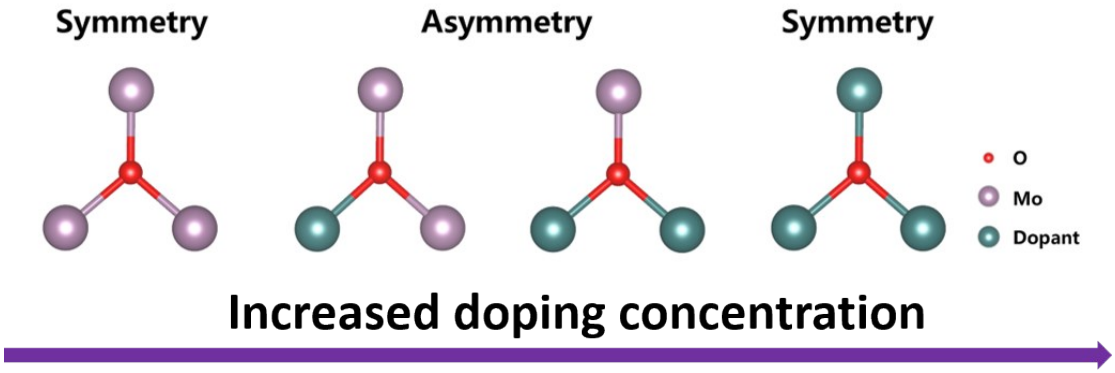

Fig. S1 Schematic illustration of introducing asymmetric local structure in MoO_2.

Based on highly ordered mesoporous MoO_2, appropriate amount of heteroatoms-doping is utilized to enhance its stability of physical structure without excessively compromising its electrical conductivity and achieve the asymmetric local sites with tuned electronic structures as well as optimal defects, consequently leading to the facilitated intrinsic electrochemical properties. With the increasing of doping concentration, new symmetric clusters, M–O–M (M=Fe, Co, Ni), will instead the desirable asymmetric bonding situation, M–O–Mo (M=Fe, Co, Ni). Such new symmetric coordination of cations displays less reactive in redox reactions compared with asymmetric ones because it not only impedes the formation of favorable disordered electronic environment but also breaks down the balance of "easy come, easy go".[6] Moreover, superfluous doping also has bad effect on the electrical conductivity. Therefore, small amount of doping is more likely to satisfy our requirements.

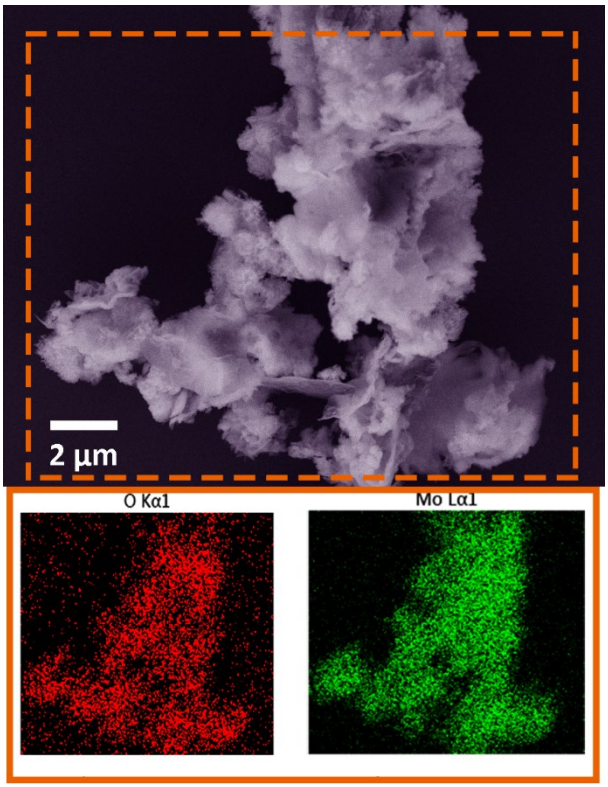

Fig. S2 SEM image and EDS mapping of Bulk-MoO_2.

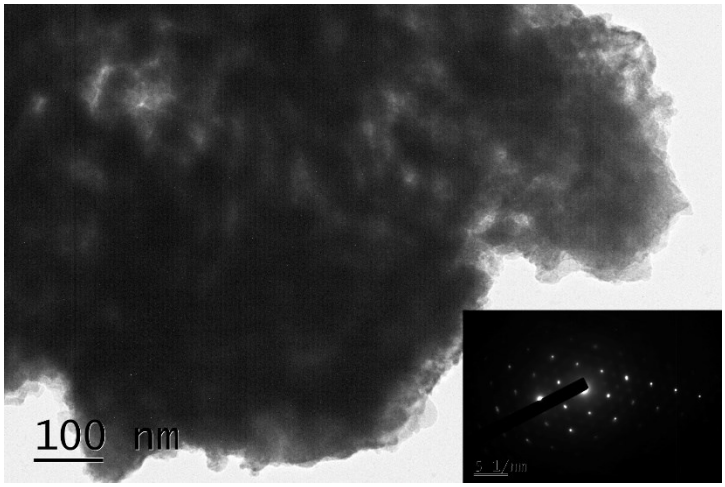

Fig. S3 TEM image and SAED pattern of Bulk-MoO_2.

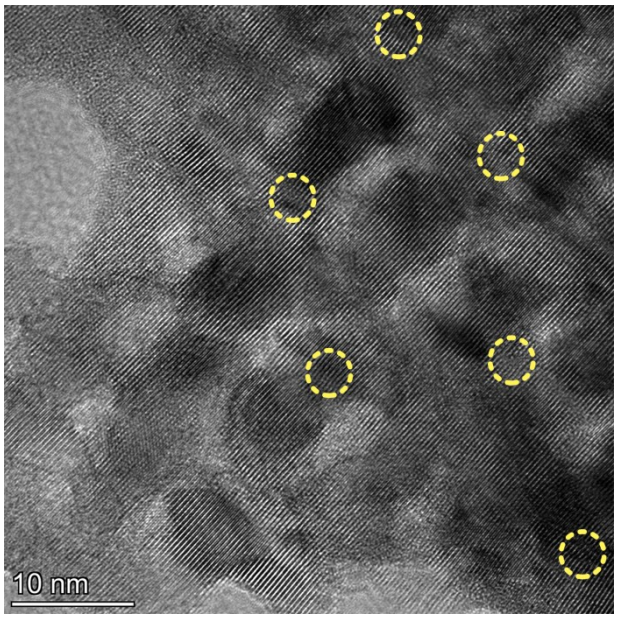

Fig. S4 HRTEM images of Meso-1%Ni-MoO_2.

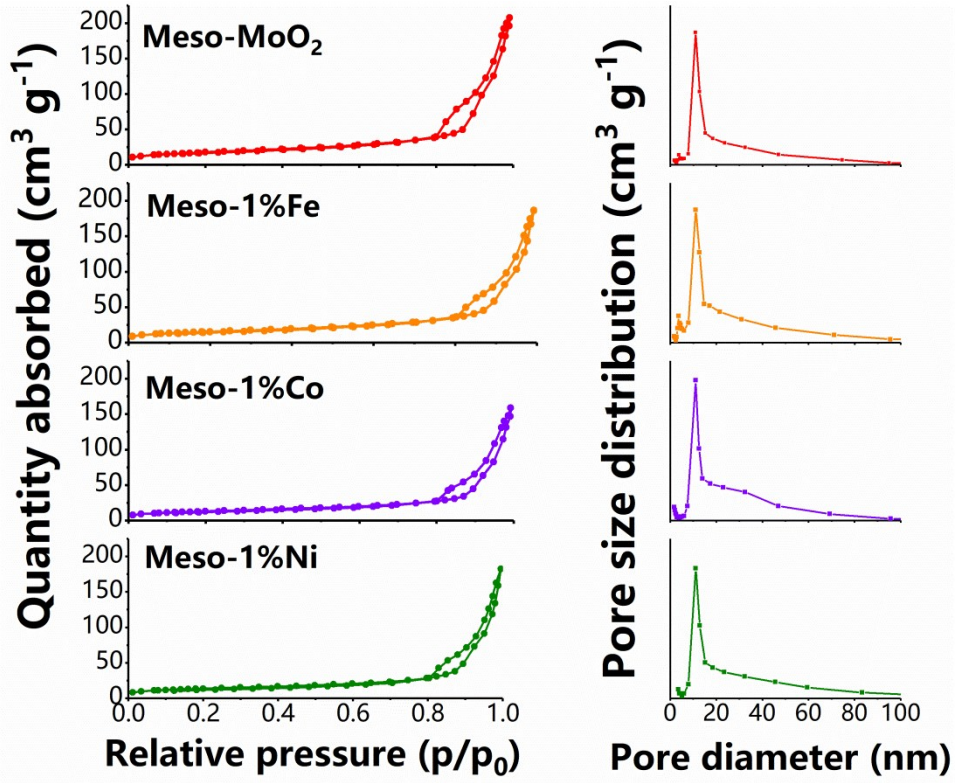

Fig. S5 N_2 sorption isotherms and pore size distributions of Meso-MoO_2, Meso-1%Fe-MoO_2, Meso-1%Co-MoO_2 and Meso-1%Ni-MoO_2.

Brunauer, Emmett, and Teller (BET) method is utilized to obtain the N_2 sorption isotherms and pore size distributions of catalysts. Accordingly, all the mesoporous samples display similar characteristic of a type IV isotherm and well-distributed pore sizes obtained from the desorption branch of isotherms, corresponding to mesoporous materials, further demonstrating the successful use of KIT-6 hard templating method in the process of preparing catalysts. The peaks located at ~11 nm also clearly illuminate the specific mesoporous structure of KIT-6 type materials, and the pore size is in agreement with the TEM images.[7,8] KIT-6 displays a 3D bicontinuous channel network with a cubic symmetry and space group *Ia3d*, thus there are two separated mesopores systems with no cross point in this template.[9] While during the synthesis of Meso-MoO_2, only half of the nanochannels systems are replicated, which may be caused by the destruction of inter-pore channels when crystal growing under high temperature.[10] Owing to a lack of complete enantiomeric pair, such type of materials tends to exhibit larger pore size after removing the KIT-6 template.[11] Notably, mesoporous nanostructures endow Meso-MoO_2 with a large specific BET surface area of 63.13 $m^2 g^{-1}$ and pore volume of 0.25 $cm^3 g^{-1}$.

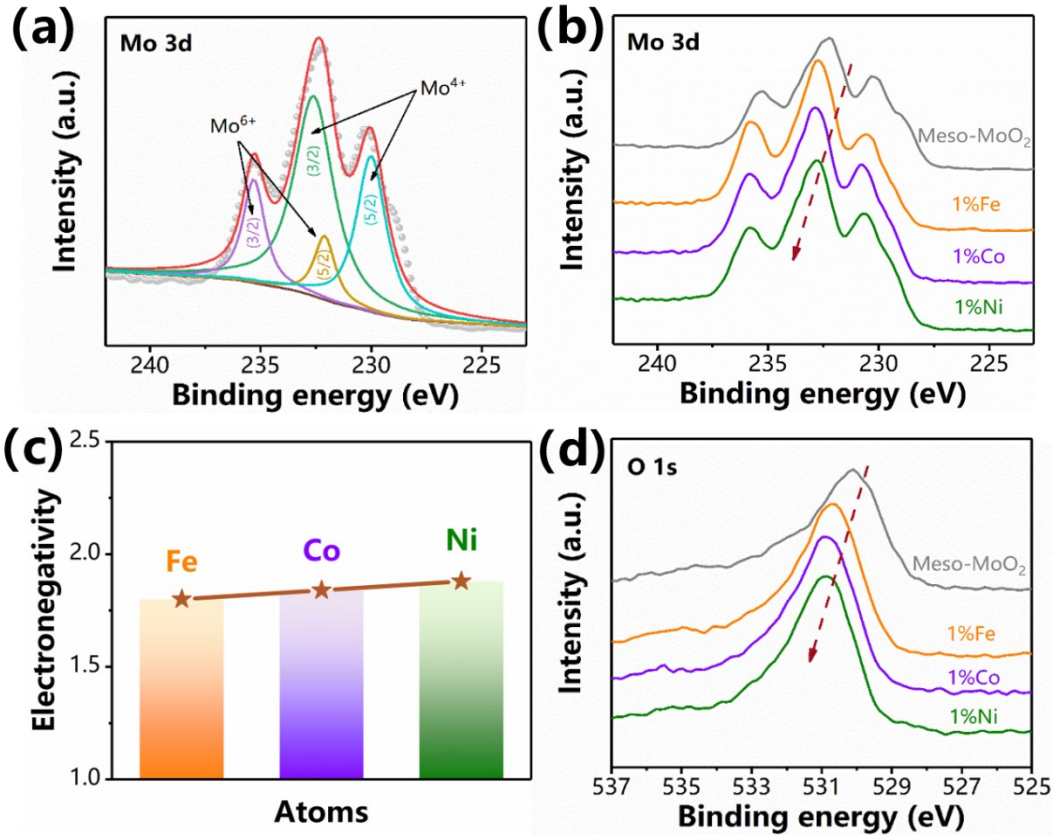

Fig. S6 (a) Mo 3d XPS spectrum of Meso-MoO_2. (b) Mo 3d XPS spectra and (d) O 1s spectra of Meso-MoO_2, Meso-1%Fe-MoO_2, Meso-1%Co-MoO_2 and Meso-1%Ni-MoO_2. (c) Electronegativities of Fe, Co and Ni on Pauling units scale.

X-ray photoelectron spectroscopy (XPS) is carried out to explore the variation of valence state of Mo and O. Fig. S6a shows the core-level spectrum of Mo 3d that splits into Mo $3d_{3/2}$ and Mo $3d_{5/2}$ peaks. The peaks of Mo^{6+} may be resulted from the slight surface oxidation of MoO_2 in air.[12] Because of the almost coincidence between the Mo $3d_{5/2}$ peak of Mo^{6+} and the Mo $3d_{3/2}$ peak of Mo^{4+}, a typical three-peak shape of Mo 3d can be determined at ~230.0, ~232.4, and ~235.4 eV.[13,14] With the substitution of Fe, Co, and Ni elements, respectively, the Mo 3d peaks and O 1s peaks are distinctly shifted to higher binding energies at different degrees (Fig. S6b and S6d), manifesting the increased valence state and reduced electron densities of Mo.[15] In addition, the shift degree is accordant with the increasing of electronegativity among Fe, Co, and Ni atoms, which is in line with the DFT results of charge density distribution (Fig. S6c).[15,16] Notably, M–O–Mo (M=Fe, Co, Ni) asymmetric structures

can form and oxygen vacancies more likely create to compensate the charges through low-valence heteroatom-doping, which is regarded as intrinsic active sites.[17,18] Meanwhile, electron deficiency on neighboring O atom sites caused by the movement of electrons from O to metal atoms can lead to the electronic reconfiguration and modulated coordination environment as well as stronger electron interactions, which is beneficial to both enhancement of intrinsic electrocatalytic activity and optimization of the binding energy of intermediates.[19,20]

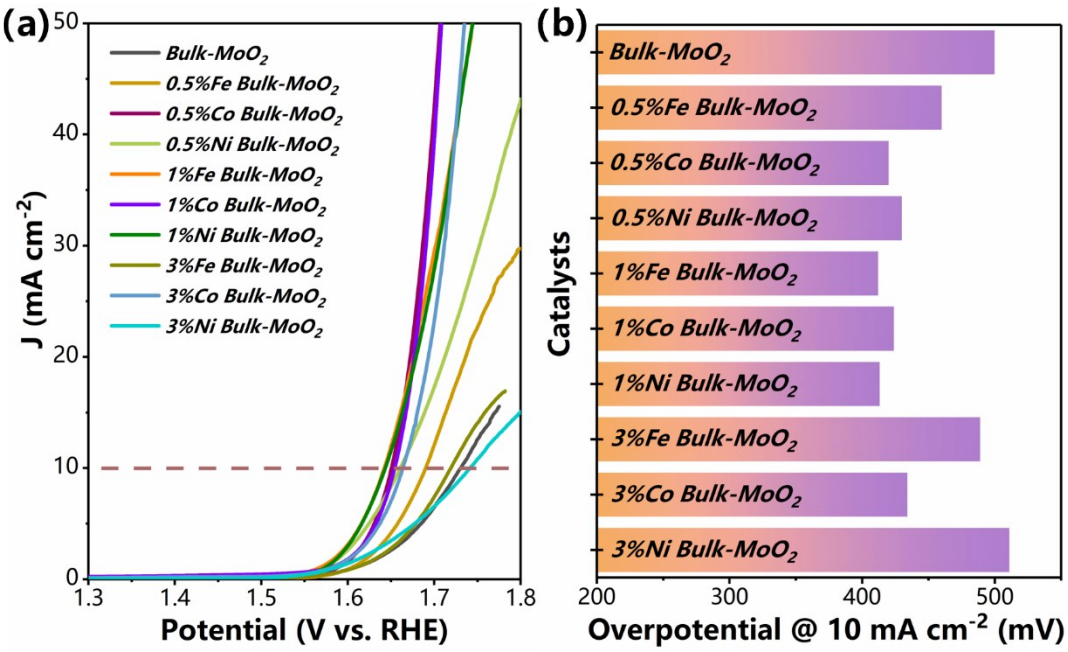

Fig. S7 (a) LSV polarization curves of Bulk-MoO_2 and corresponding doping ones. (b) Comparison of the overpotentials at the current density of 10 mA cm^{-2}.

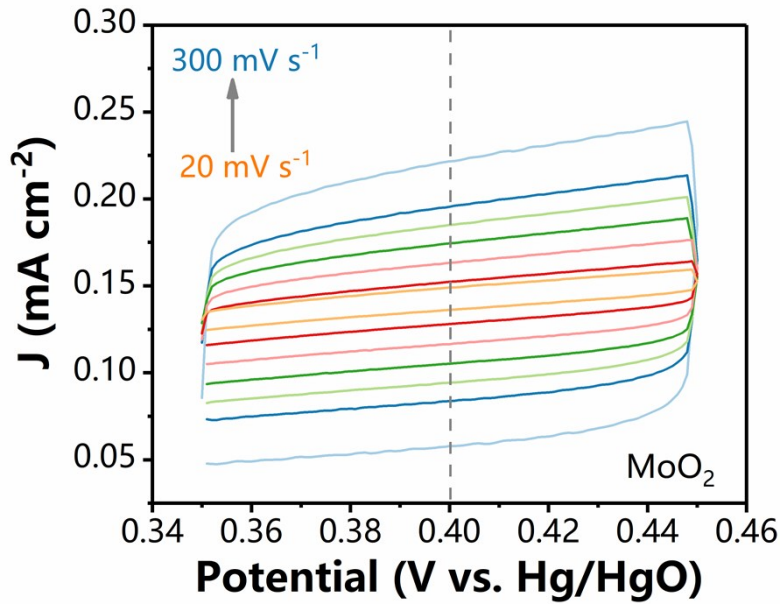

Fig. S8 Cyclic voltammograms curves of Bulk-MoO_2 at the scan rate range of 20 ~ 300 mV s^{-1}.

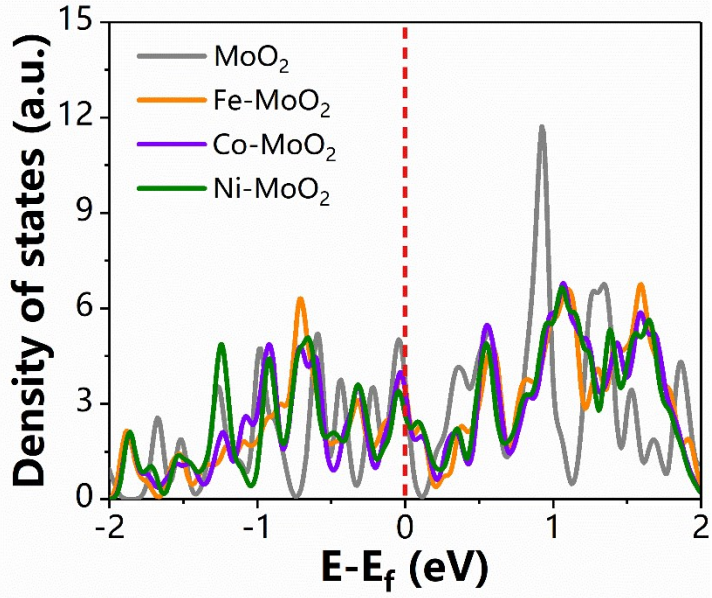

Fig. S9 DOS of MoO_2, Fe-MoO_2, Co-MoO_2 and Ni-MoO_2.

Density of states (DOS) of pure MoO_2 and metal-doping ones are calculated to further investigate the influence of foreign atoms. Remarkably, as a type of unusual metal oxides, MoO_2 resides across the Fermi level, presenting a metallic-like electrical conductivity, which is beneficial to the electrochemical properties. When heteroatoms (Fe, Co, Ni) substitute Mo atoms with low concentration respectively, Fermi level is modulated while DOS still shows no energy gap near the Fermi level, even though the conductivity displays a slight decrease. The decline of conductivity is resulted from additional scattering center of charge carriers caused by the incorporation of foreign ions, which decreases the mean free path of charge carriers.[21] Actually, its metallic behaviors are not excessively changed after low concentration metal-incorporating.

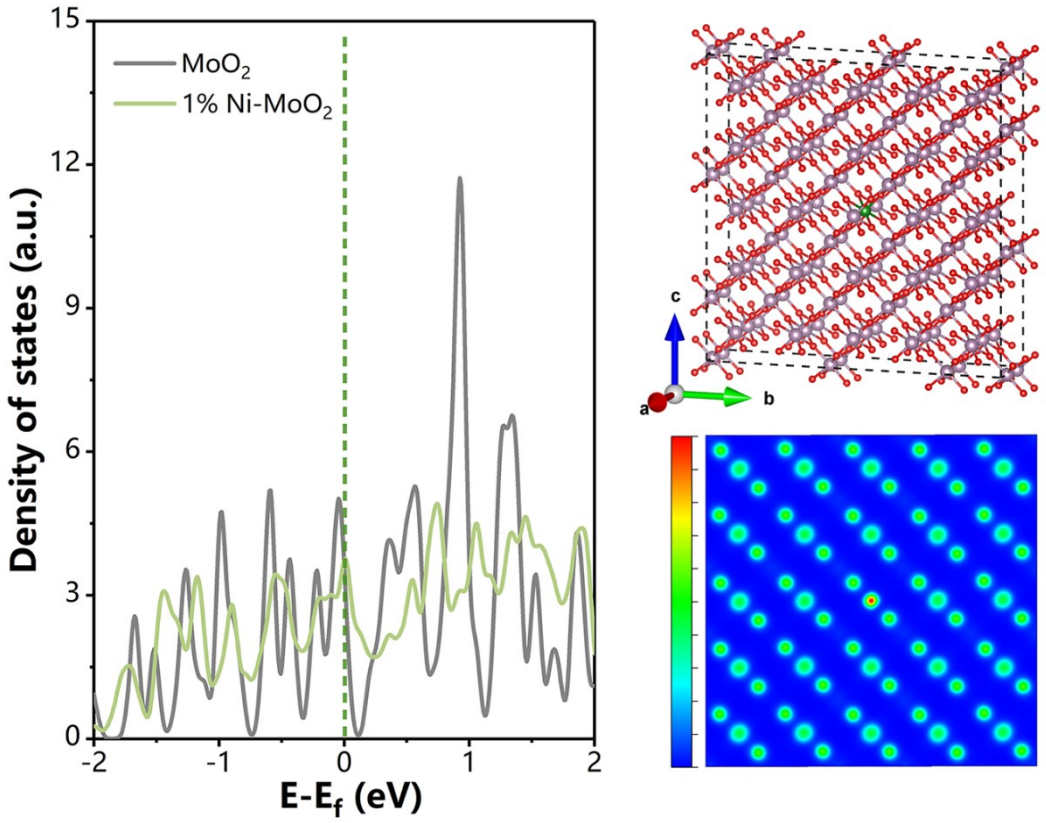

Fig. S10 DOS of MoO_2 and 1%Ni-MoO_2 with corresponding charge density mapping.

DOS of 1%Ni-MoO_2 are performed more precisely in Fig. S10, and similar results can be found that it still presents the unusual metallic-like electrical conductivity. And the charge density distribution also displays an obvious electron transfer between O and Ni.

Table S1 Electronegativities of Mo, Fe, Co and Ni on Pauling units scale.[15,16]

Atom	Mo	Fe	Co	Ni
Electronegativity	1.47	1.80	1.84	1.88

Table S2 Electronegativities of Mo, Fe, Co and Ni on Allred-Rochow scale.[16]

Atom	Mo	Fe	Co	Ni
Electronegativity	1.30	1.64	1.70	1.75

Table S3 Bond length (BL) and bond angle (BA) of MoO_2 and 1%Ni-MoO_2.

Electrocatalyst	BL1/Å	BL2/Å	BL3/Å	BA1/°	BA2/°	BA3/°
MoO_2	1.98592	2.05140	2.05140	138.1653	138.1653	83.6644
1%Ni-MoO_2	1.90580	2.11671	1.99565	129.9077	144.7207	85.3702

References

[1] G. Kresse and J. Furthmüller, *Comp. Mater. Sci.*, 1996, **6**, 15-50.

[2] G. Kresse and J. Hafner, *Phys. Rev. B*, 1993, **47**, 558.

[3] J. P. Perdew, J. Chevary, S. Vosko, K. A. Jackson, M. R. Pederson, D. Singh and C. Fiolhais, *Phys. Rev. B*, 1992, **46**, 6671.

[4] J. P. Perdew, K. Burke and M. Ernzerhof, *Phys. Rev. Lett.*, 1996, **77**, 3865.

[5] P. E. Blöchl, *Phys. Rev. B*, 1994, **50**, 17953.

[6] K. Yu, D. Lei, Y. Feng, H. Yu, Y. Chang, Y. Wang, Y. Liu, G. Wang, L. L. Lou, S. Liu and W. Zhou, *J. Catal.*, 2018, **365**, 292-302.

[7] X. Li, J. Shao, J. Li, L. Zhang, Q. Qu and H. Zheng, *J. Power Sources*, 2013, **237**, 80-83.

[8] T. Grewe, X. Deng and H. Tüysüz, *Chem. Mater.*, 2014, **26**, 3162-3168.

[9] F. Kleitz, S. H. Choi and R. Ryoo, *Chem. Commun.*, 2003, **17**, 2136-2137.

[10] C. Dickinson, W. Zhou, R. P. Hodgkins, Y. Shi, D. Zhao and H. He, *Chem.*

Mater., 2006, **18**, 3088-3095.

[11] Y. Shi, B. Guo, S. A. Corr, Q. Shi, Y. S. Hu, K. R. Heier, L. Chen, R. Seshadri and G. D. Stucky, *Nano Lett.*, 2009, **9**, 4215-4220.

[12] X. Chen, Z. Zhang, X. Li, C. Shi and X. Li, *Chem. Phys. Lett.*, 2006, **418**, 105-108.

[13] Y. Jin, H. Wang, J. Li, X. Yue, Y. Han, P. K. Shen and Y. Cui, *Adv. Mater.*, 2016, **28**, 3785-3790.

[14] B. Brox and I. Olefjord, *Surf. Interface Anal.*, 1988, **13**, 3-6.

[15] H. Zeng, S. Chen, Y. Q. Jin, J. Li, J. Song, Z. Le, G. Liang, H. Zhang, F. Xie, G. Chen, Y. Jin, X. Chen and H. Meng, *ACS Energy Lett.*, 2020, **5**, 1908-1915

[16] J. B. Mann, T. L. Meek, E. T. Knight, J. F. Capitani and L. C. Allen, *J. Am. Chem. Soc.*, 2000, **122**, 5132-5137.

[17] R. D. Shannon and Acta Crystallogr., *Sect. A: Cryst. Phys., Diffr., Theor. Gen. Crystallogr.*, 1976, **32**, 751-767.

[18] J. Paier, C. Penschke and J. Sauer, *Chem. Rev.*, 2013, **113**, 3949

[19] J. Chen, Q. Zeng, X. Qi, B. Peng, L. Xu, C. Liu and T. Liang, *Int. J. Hydrog. Energy*, 2020, **45**, 24828-24839.

[20] B. Qiu, L. Cai, Y. Wang, X. Guo, S. Ma, Y. Zhu, Y. H. Tsang, Z. Zheng, R. Zheng and Y. Chai, *Small*, 2019, **15**, 1904507.

[21] J. F. Shackelford, *Introduction to Materials Science for Engineers*, Prentice Hall, Englewood, 2009.